Fluctuations in Rotation Rate of the Flagellar Motor of *Escherichia coli*

Michael Kara-Ivanov, Michael Eisenbach, and S. Roy Caplan
Department of Membrane Research and Biophysics, The Weizmann Institute of Science, 76100 Rehovot, Israel

ABSTRACT The purpose of this work was to study the changes in rotation rate of the bacterial motor and to try to discriminate between various sources of these changes with the aim of understanding the mechanism of force generation better. To this end *Escherichia coli* cells were tethered and videotaped with brief stroboscopic light flashes. The records were scanned by means of a computerized motion analysis system, yielding cell size, radius of rotation, and accumulated angle of rotation as functions of time for each cell selected. In conformity with previous studies, fluctuations in the rotation rate of the flagellar motor were invariably found. Employing an exclusively counterclockwise rotating mutant ("gutted" RP1091 strain) and using power spectral density, autocorrelation and residual mean square angle analysis, we found that a simple superposition of rotational diffusion on a steady rotary motion is insufficient to describe the observed rotation. We observed two additional rotational components, one fluctuating (0.04–0.6 s) and one oscillating (0.8–7 s). However, the effective rotational diffusion coefficient obtained after taking these two components into account generally exceeded that calculated from external friction by two orders of magnitude. This is consistent with a model incorporating association and dissociation of force-generating units.

GLOSSARY

D	rotational diffusion coefficient (Eq. 1)
$D(t)$	time-dependent rotational diffusion coefficient (Eq. 7)
D_∞	limiting value of rotational diffusion coefficient (Eq. 7)
D_f	diffusion coefficient calculated from the frictional coefficient
$D_{\alpha=1}$	rotational diffusion coefficient judged from initial slope of the plot $\sigma^2_{\alpha\tau}$ vs α
K_d	dimensionless dissociation constant (Eq. 16)
$K(t)$	rotation rate autocorrelation function
K_0	preexponential factor of the rotation rate autocorrelation function
k_1	pseudo-first-order rate constant for binding of force-generating units
k_2	rate constant for release of force-generating units
m	number of associated force-generating units
n	overall number of force-generating units
PSD	power spectral density
p	probability of a single unit being found in the associated state
r^2	coefficient of determination
T	time correlation constant characterizing the memory of the system
T_m	length of the time interval representing one realization in an ensemble
t	time
α	number of revolutions
$\theta(t)$	accumulated angle describing position of bacterial cell
$\Delta\theta(t)$	residual accumulated angle (Eq. 2)
σ	standard deviation of the rotation rate
σ_{loc}	standard deviation of the local rotation rate
σ_{sys}	standard deviation of the rotation rate arising from the noise of the measuring system
$\sigma^2_{\alpha\tau}$	the variance of the time interval $\alpha\tau$ necessary to accomplish α revolutions (Eq. 1)
τ	mean rotation period
$\Omega(t)$	deviation from average rotation rate (Appendix A)
$\omega(t)$	rotation rate
$\overline{\omega(t)}$	average rotation rate
ω_0	rotation rate of the rotor with a single associated force-generating unit

INTRODUCTION

The motor responsible for the spinning motion of a single bacterial flagellum couples a transmembrane flux of cations (usually protons) to mechanical rotation of a rotor supported within a stator. Both the structural and the functional aspects of a molecular rotational mechanism present a formidable array of problems, many of which are as perplexing now as they were two decades ago when Berg and Anderson (1973) first showed that bacteria swim by rotating their flagella. The development of the technique of tethering bacteria (Silverman and Simon, 1974) permitted direct observation and measurement of the rotation of a single motor by observing the motion of an entire bacterial cell. Using this method, Berg attempted to determine whether the motor has a ratchet-like or continuous drive by following the rotation with a tracking microscope and pinhole technique (Berg, 1974, 1976; Berg et al., 1982). The eventual conclusion was that the motion is surprisingly smooth even after taking elastic filtering by the tether into account and that the

Received for publication 20 December 1994 and in final form 20 April 1995.

Address reprint requests to Dr. S. Roy Caplan, Weizmann Institute of Science, Dept. of Membrane Research and Biophysics, 76100 Rehovot, Israel. Tel: (972)-8-343924; Fax: (972)-8-344112; E-mail: bmcapln1@weizmann.weizmann.ac.il.

0006-3495/95/07/250/14 $2.00

number of steps (if present) could not be less than 100 per revolution (Berg et al., 1982).

Nevertheless the rotation is not completely smooth. A systematic study of fluctuations in the period of revolution by Khan et al. (1985) led to the conclusion that the motor is free to execute rotational Brownian movement above a certain energy threshold. Khan et al. also concluded that "apart from the discontinuous steps . . . and the long-term drifts . . . fluctuations attributable to torque generation were not evident". However, Eisenbach et al. (1990) observed fluctuations in the rotation rate that could not be attributed to simple rotational Brownian movement. Fluctuations in flagellar rotation were also observed in nontethered flagella, although on a smaller time scale (Kudo et al., 1990). As the fluctuations are still in need of explanation, and might well be an important clue to the mechanism of the rotary machinery at the molecular level, we have investigated them more rigorously. Here we report the results of this investigation. They suggest that the probable source of the fluctuations is loose binding of force-generating units to the rotor.

MATERIALS AND METHODS

Chemicals

Antibodies to flagellin were from the National Center for Enterobacteriaceae, Central Laboratories, Ministry of Health, Jerusalem, Israel. Other chemicals were of analytical grade. Ficoll 400 was obtained from Sigma Chemical Co. (St. Louis, MO).

Bacteria

The *E. coli* strains used in this study were RP1091 and RP3098 (Parkinson and Houts, 1982) and RP437 (Parkinson, 1978). The cells were grown at 35°C in a tryptone broth. Afterwards the cells were washed and resuspended in 10 mM potassium phosphate (pH 7)/0.1 mM EDTA/5 mM glycerol before experimentation.

Data acquisition

Flagellar rotation was assayed by the tethering technique (Silverman and Simon, 1974). Most of the flagella of the RP1091 and RP437 cells were sheared off by a blender, and the cells were subsequently tethered on to a cover glass (Lapidus et al., 1988) by using *flil* preadsorbed antibodies against flagellin as described earlier (Ravid and Eisenbach, 1983). RP3098 cells were attached to a cover glass by antibodies against the cell surface. Data were collected by recording videotapes (50 noninterlaced fields/s) of tethered cells in a flow chamber (Berg and Block, 1984) under a Zeiss phase-contrast microscope. The initial flow medium was the potassium phosphate-EDTA-glycerol suspending medium described above. The flow of the liquid in the flow chamber was stopped or minimized during the periods of recording. To maintain constant temperature, the flow chamber filled with initial medium was placed on a temperature-regulated microscope stage controlled by circulation of water from a thermostatted water bath. New medium reaching the flow chamber had been kept in the same water bath. Measurements were performed at 29°C. The size, angular position, and average radius of rotation of a given cell body were determined by using the motion analysis system described below.

Cells that slowed down or paused at fixed angles were disregarded because of suspected mechanical interaction with the glass. After the initial collection of data from selected cells, the flow medium was usually changed by addition of a viscous agent (stepwise change in Ficoll concentration) or by the addition of uncoupler (stepwise change in 2,4-dinitrophenol (DNP) concentration). In experiments involving increased viscous loads, Ficoll was added to the medium from concentrated stock solutions. Viscosity was measured in Ostwald and Ubbelohde viscometers at 29.0°C. In each case 7000 bacterial images were accumulated, 1 every 20 ms. Operation of a peristaltic pump (LKB 2232 Microperpex S, flow rate 30–40 ml/h) for 6–10 min changed the contents of the flow chamber.

Motion analysis system

The main features of the system are:

(1) Stroboscopic illumination with brief (2–5 μs) light flashes, providing a sharply defined image of some 60 pixels in each field (a synchronized bulb-type xenon lamp was used in combination with a high resolution camera mounted on a Zeiss microscope).
(2) Appropriate filtering and processing techniques, improving the signal-to-noise ratio.
(3) Computerized field-by-field data acquisition, with program-controlled videotapes.
(4) Continuous automatic measurement of bacterial size, angular position, positions of the center of gravity and center of rotation, etc., at discrete time intervals of 20 ms, by approximating the cell body as an equivalent ellipsoid.
(5) Processing of raw data by a dedicated computer application designed to calculate accumulated angle, angular velocity, and other descriptive parameters.
(6) Visual display of calculated data on a monitor, enabling them to be edited and filed for further processing by external statistical or other programs.

The system was designed and built in collaboration with Arshach Applied Science Laboratories (Rosh-Pinna, Israel).

Calibration and testing of the system

Calibration and testing were carried out in part by constructing several types of fake cells, i.e., cardboard cut-outs of typical cell shapes as seen in the microscope. To ensure absolutely smooth rotation, fake cells were attached to a massive turntable (Lenco, 3 kg) mounted on vibration dampers and spun by means of a rubber-tired transmission wheel. Efforts were taken to ensure that the contrast between fake cell and surroundings simulated as far as possible that of real tethered cells. The mean rotation rate of a fake cell within the physiological range was correctly determined by our system by using the method of least squares. An estimated standard error of slope determination (see, for example, Ott, 1988) was less than ±0.01%. The angular reading error (i.e., standard deviation) associated with the system, σ_{read}, was determined with tethered cells from several hundred independent measurements of the long axis angular position for a given frame. Using a number of arbitrarily chosen frames from different experiments, we found $\sigma_{read} = \pm 1.50–3.31°$, depending on the shape and length of the tethered bacterial cell. This error arises from uncertainties in the cell image boundary definition in regions where the contrast is low. Thus, in the measurement of rotation rate from any given pair of adjacent frames, the standard deviation arising from the system, σ_{sys}, is given by $\sigma_{sys} = (2^{1/2}/0.02)\sigma_{read} = \pm 0.29–0.65$ Hz. Note that small changes in cell shape from frame to frame are averaged out by our algorithms.

To estimate the restricted (nonrotational) Brownian motion or jiggling of the cell body resulting from collisions with medium molecules, RP3098 cells were tethered to the glass by antibody to the cell surface. These cells carry a deletion of the entire *flil-fliH* region (Parkinson and Houts, 1982) and thus lack all motor and flagella components.

Point dark-field microscopy

This method measures local submicron cell membrane displacements within the frequency range 0.3–15 Hz. The measurements were performed

in collaboration with Prof. R. Korenstein and co-workers by using a technique recently developed in their laboratory (Levin and Korenstein, 1991; Mittelman et al., 1991). Tethered cells, attached to a glass coverslip by antibody to the flagellin (RP1091) or to the cell surface (RP3098), were illuminated over a small area (0.25 μm^2), and the time-dependent changes in light reflection and scattering were recorded.

Calculation of the frictional coefficient of the bacterial body

To estimate the frictional coefficient f of a rotating tethered cell we treated the cell body as a prolate ellipsoid and used the formula $f = f_r + r^2 f_t$ where f_r is the frictional coefficient for rotation about the minor axis of the ellipsoid, f_t the frictional coefficient for translation perpendicular to the major axis of the ellipsoid, and r the distance from the point of attachment of the tether to the center of the cell (Sadron, 1953; Meister and Berg, 1987; Iwazawa et al., 1993). The diffusion coefficient D_f, calculated from the frictional coefficient for the group of RP1091 cells (typical cell size, 3 $\mu m \times 0.7$ μm; radius of rotation, 0.8 μm) according to the Einstein-Smoluchowsky relation $D_f = kT/f$, did not exceed 0.2 rad^2/s (see Table 1).

RESULTS AND DATA TREATMENT

Rotation rate versus time

An example of data obtained by our system is shown in Fig. 1 *A*. To avoid fluctuations in rotation rate resulting from reversals associated with the switch action, the study was carried out with the "gutted" strain RP1091, unless otherwise mentioned. This strain is a mutant derived from RP437 which, as a result of the deletion of the genes from *che*A to *che*Z, lacks a large part of the chemotaxis machinery (Parkinson and Houts, 1982). To calculate accumulated angles from the angular positions of the long axis of the bacterium (i.e., the raw data) two alternative algorithms were employed. The first was based on the assumption that the angle of rotation during 20 ms (one field) does not exceed 90°; i.e., successive pairs of frames always show the bacterium in the same or adjacent quadrants. This algorithm cannot be used for rapidly rotating bacteria. We limited its application to cells with average rotation rates less than 8 Hz. The second was based on a determination of the position of the instantaneous center of rotation, defined by the intersection of two lines corresponding to the positions of the long axes in two adjacent fields. This algorithm can be used for more rapidly rotating bacteria but requires that rotation of the bacterial body should occur around a point near one end, as is frequently the case, rather than around the center.

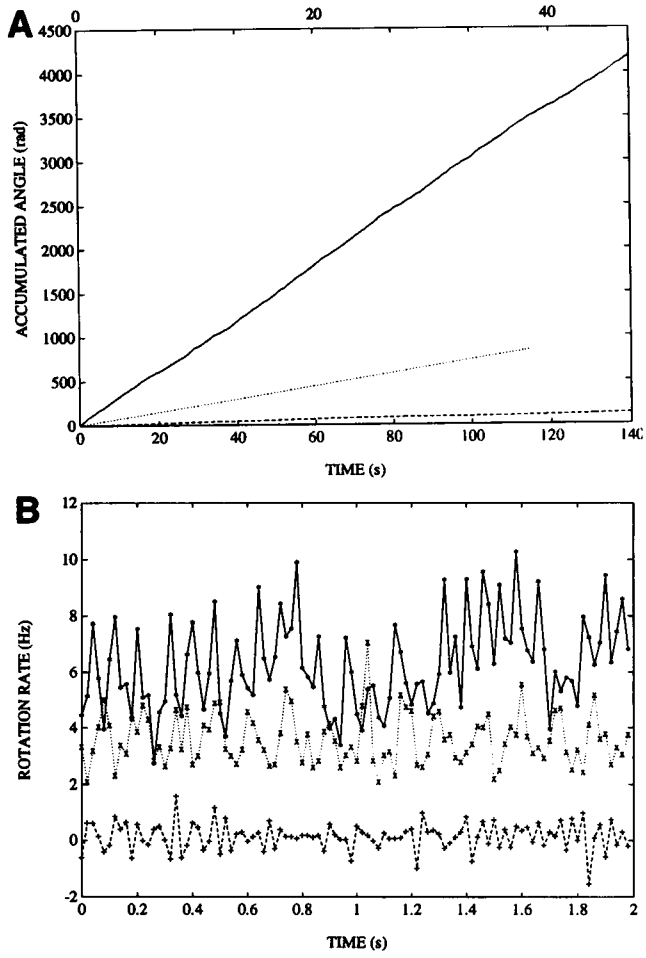

FIGURE 1 Accumulated angle and rotation rate as functions of time for a tethered E. coli cell (RP1091). (*A*) Accumulated angle, corresponding to the position of the long axis of a smoothly rotating cell versus time. Each line consists of a series of discrete points at 20-ms intervals. *Upper curve*: 0% Ficoll; the rotation rate determined by least-squares is 4.749 ± 0.001 Hz (mean ± estimated standard error). *Middle curve*: 5% Ficoll; rotation rate 3.497 ± 0.001 Hz. The time scale for this curve is shown above the plot. *Lower curve*: 20% Ficoll; rotation rate 0.144 ± 0.001 Hz. (*B*) Rotation rate versus time for 2-s time intervals selected from the data shown in *A*. *Upper curve*: 0% Ficoll; the mean rate for the selected interval is 6.25 ± 1.62 Hz (standard deviation of the local rate calculated for the 100 points shown). Oscillations are visible at twice the rotation frequency (see text). *Middle curve*: 5% Ficoll, mean rate 3.60 ± 0.90 Hz. *Lower curve*: 20% Ficoll, mean rate 0.15 ± 0.49 Hz. The amplitude of the fluctuations decreases linearly with a decrease in average rotation rate.

TABLE 1 Parameters of rotation of RP1091 *E. coli* cells

	σ (Hz)	D_f (rad^2/s)	D_∞ (rad^2/s)	T (s)
Group 1	1.92 ± 0.16	0.18 ± 0.02	17.08 ± 3.60	0.29 ± 0.03
Group 2	1.30 ± 0.26	0.17 ± 0.01	0.95 ± 0.39	0.03 ± 0.01

Values of $\overline{\omega(t)}$ (average rotation rates of tethered cells) ranged from 0.694 to 13.161 Hz for the cells in group 1 (23 cells, see text) and from 0.933 to 9.137 Hz for the cells in group 2 (7 cells). Mean ± SE (standard error of the mean) values of σ (standard deviation of the rotation rate), D_f (diffusion coefficient of the bacterial body calculated from the friction coefficient, D_∞ (limiting value of rotational diffusion coefficient), and T (time correlation constant characterizing the memory of the system) are presented for each group.

An important difference between the earlier analysis of variance of tethered cell rotation carried out by Khan et al. (1985) and the present study is that Khan et al. measured the variance of whole rotation periods whereas here the variance in field-by-field angular displacement is measured. Although much more informative, our approach required particular attention to be paid to position-dependent irregularities of rotation.

An example of the time dependence of the measured rotation rate for the cell shown in Fig. 1 *A* is shown in Fig.

1 *B*. Each point corresponds to a local rate obtained from the difference of two successive values of the accumulated angle. In the upper curve (motility buffer without Ficoll), large fluctuations are seen, predominantly oscillations at twice the rotation frquency. The origin of these is discussed in the next section. The standard deviation of the local rate, σ_{loc}, calculated for the 100 data points shown in Fig. 1 *B*, is ± 1.62 Hz, which is ~30% of the mean rate. Only a minor part (not more than 20%) of these fluctuations can be attributed to the noise of the measuring system. This estimate was made on the basis of a detailed analysis of various noise components introduced by the system. It turned out that σ_{sys}, which is ± 0.30 Hz for this particular cell, is the dominant component.

To determine the effect of increased viscosity on the fluctuations, the experiment was repeated in various Ficoll concentrations. The value of σ_{loc} (which is a measure of the amplitude of the rate fluctuations) decreased upon increase of the Ficoll concentration. A similar pattern was seen after a stepwise increase of DNP concentration up to 5 mM (not shown). The general trend observed was a linear decrease in σ_{loc} with decrease in the mean rotation rate in both cases.

Distributions of angular positions of rotating cells in the angular and frequency domains

It seems possible that if a relatively small number of equally spaced force-generating units are located near the perimeter of the rotor (see, for example, Khan et al., 1988; Caplan and Kara-Ivanov 1993), a periodic pattern in the histogram of angular positions might be observed. Using the fast Fourier transform method, we analyzed histograms of thousands of angular positions for patterns without success. Another approach was to apply PSD analysis to the time dependence of the rotation rate. However, no peaks were found in the power density spectrum in the region 2–25 Hz (see Figs. 2 and 3 *B*), except that in most cases distinct peaks exactly corresponding to multiples of the mean rotation rate were observed. A geometrical analysis of the rotation indicated that these peaks, which usually appear as doublets, arise partly because of lack of parallelism between the plane of rotation and the coverslip and partly because the axis of rotation may be viewed somewhat obliquely, leading to an apparent acceleration and deceleration in each revolution. They provide a sensitive tool for the determination of the mean rotation rate and its distribution about the mean.

Our results indicate that no statistically significant high frequency pattern is observable at the resolution of our equipment in either the angular or frequency domains. Assuming an absolutely rigid tether, our technique can resolve up to 25 equidistant steps per second if the rotation rate is constant. Hence we are still in agreement with the conclusions of Berg et al. (1982) that, even if the rotation of the motor does have a stepping character, the number of steps is

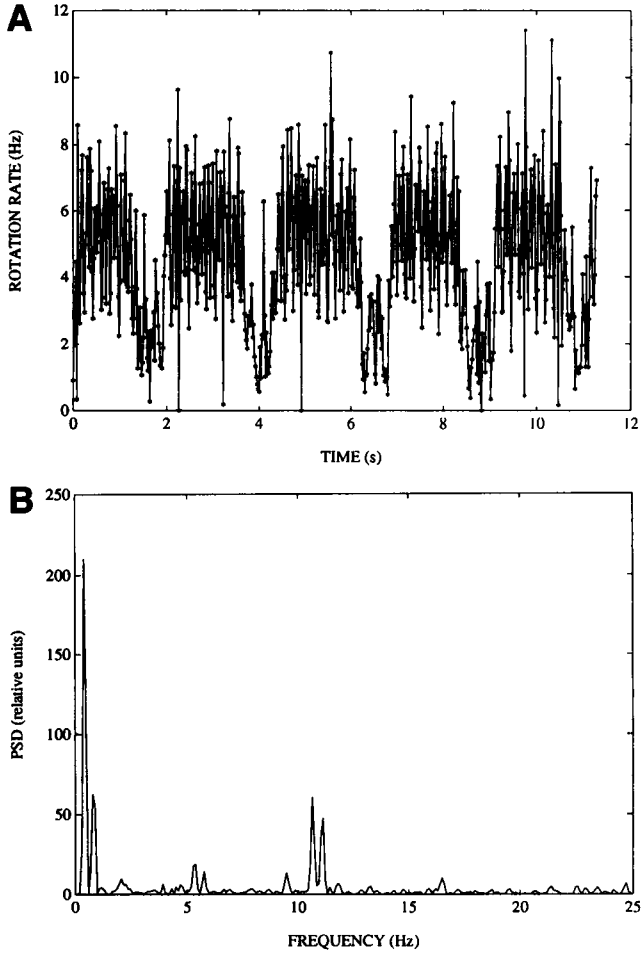

FIGURE 3 Rotation rate as a function of time for a tethered *E. coli* cell (RP1091) with its associated power spectral density. (*A*) Rotation rate versus time over an extended period. Distinct oscillations in rate are seen. (*B*) Power spectral density of the data in *A* showing an oscillatory component at approximately 0.4 Hz. The doublet peaks at 5.5 Hz and 11 Hz correspond, respectively, to the rotation rate and double the rotation rate and are discussed in the text.

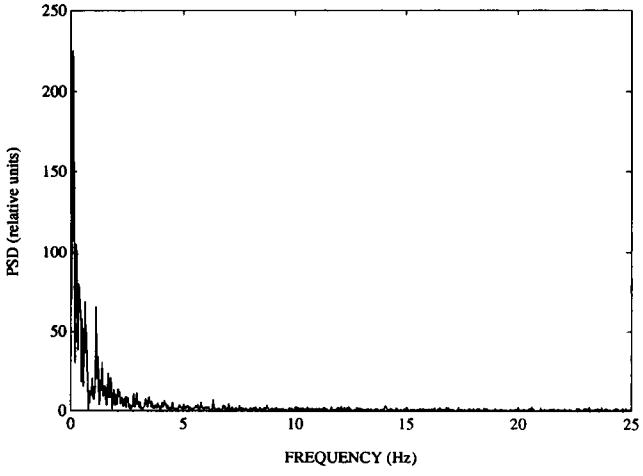

FIGURE 2 Power spectral density of the rotation rate for a tethered RP1091 cell. Peaks corresponding to slow oscillations of rate are present in the low frequency region of the spectrum. In contrast to the cell studied in Fig. 1, this cell did not show oscillations at multiples of the rotation rate.

too large to be resolved with current methods. This does not conflict with the postulated regular distribution of force-generating units, as elastic filtering may well conceal a pattern in the distribution of positions.

Slow changes in rotation rate

In more than 60% of the RP1091 cells studied, a slow change in rotation rate (approximately once in 1–6 s) between a faster and a slower component was visible by eye. A typical PSD of the rotation rate for RP1091 cells is shown in Fig. 2. The peaks in the low frequency region of the spectrum are related to the slow changes of rotation rate, the latter being usually (but not always) visually identifiable by videotape inspection. For several of these cells the changes had a clearly periodic character, as is seen in the example shown in Fig. 3. In this case the fast phase lasted 1.5 s and the slow phase lasted 0.8 s on the average. Obviously these oscillations cannot be the consequence of mechanical interaction of the cell body with the glass surface. Of 37 RP1091 cells studied, 24 (65%) had at least one peak in the low frequency (0–1.2 Hz) region of the power spectrum. Most frequently the maximal peaks were located between 0.16 and 0.3 Hz. No significant alteration in the location of the maxima was seen on changing solution viscosity, nor was any cross-correlation observed between the oscillations and the rotation.

Behavior similar to that shown in Fig. 2 was also observed in the group of RP437 (wild type for chemotaxis) cells studied. Low frequency peaks were found in six of the seven cells examined. To investigate the possible effect of attractant stimulation on low frequency oscillations, a mixture of methylaspartic acid (0.1 mM) and aminoisobutyric acid (10 mM) was added to the flow medium. Two cells lost their low frequency peaks and the remainder were unaffected. Although no firm conclusion can be drawn from this experiment, the low frequency phenomenon seems insensitive to attractant stimulation.

It should be mentioned that we observed a remarkable resemblance between the respective time scales of the fast and slow phases in the rotation of the RP1091 cells and the clockwise and counterclockwise phases in the RP437 cells (not shown).

Data treatment according to the method of Khan et al. (1985)

Although our data contain a great deal of detailed information on the successive angular positions of the bacterial body during a single revolution, for comparison with previous work we performed a preliminary zero level analysis. This made use of smoothed data obtained by averaging the rotation rate for each revolution. A program was written to calculate the lengths of periods of successive revolutions from the accumulated angle time dependence. Linear interpolation provided the missing data in the small time intervals at the beginning and end of each revolution. This treatment converted our data to the form of the raw data used by Khan et al. (1985) to prove that tethered *Streptococcus* cells are free to execute rotational Brownian movement. According to Khan et al. (1985), if this is the case the variance of the time interval $\alpha\tau$ necessary to accomplish α revolutions of mean period τ is proportional to α:

$$\sigma^2_{\alpha\tau} = (D\tau^3/(2\pi^2))\alpha\,, \qquad (1)$$

where D is the diffusion coefficient for rotational Brownian movement. Plots of the variance $\sigma^2_{\alpha\tau}$ as a function of α for two RP1091 cells are shown in Fig. 4. Khan et al. (1985) found a pronounced nonlinearity for *Streptococcus* cells and restricted themselves to the initial slopes, presenting diffusion coefficient values $D_{\alpha=1}$ calculated from the slopes evaluated at $\alpha = 1$. They explained the upward curvature of their plots as stemming from a gradual decrease of the rotation rate (such increases and decreases were referred to as drift). Values of $D_{\alpha=1}$ for the two RP1091 cells depicted in Fig. 4 were 7.23 and 33.06 rad^2/s (upper and lower curves, respectively). These values significantly exceed the values D_f = 0.19 and 0.22 rad^2/s, calculated from the frictional coefficients of ellipsoids with dimensions corresponding to those of the RP1091 cells. An interpretation of these data will be discussed below.

Autocorrelation function of rotation rate

An important tool in the study of stochastic processes is the autocorrelation function (see, for example, Cooper and McGillem, 1967). A typical autocorrelation function of the rotation rate of a tethered bacterium sampled with a time interval of 20 ms is shown in Fig. 5. An initial rapidly decreasing component is seen, followed by a series of small

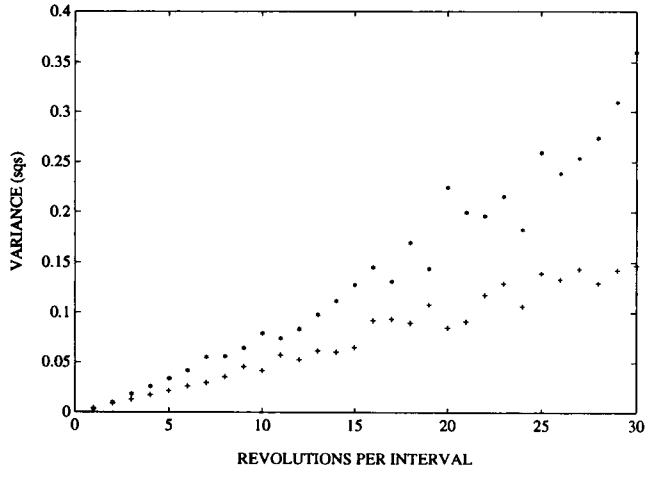

FIGURE 4 Variance in rotation interval as a function of the number of revolutions per interval for two medium-sized *E. coli* cells (RP1091) calculated according to the algorithm of Khan et al. (1985). The mean rotation periods for the first (*) and second (+) cells, respectively, were 0.209 and 0.095 s. The rotational diffusion coefficients $D_{\alpha=1}$ for the two cells calculated from the initial slopes of the curves (using the data points at $\alpha = 1$) were 7.23 and 33.06 rad^2/s, respectively.

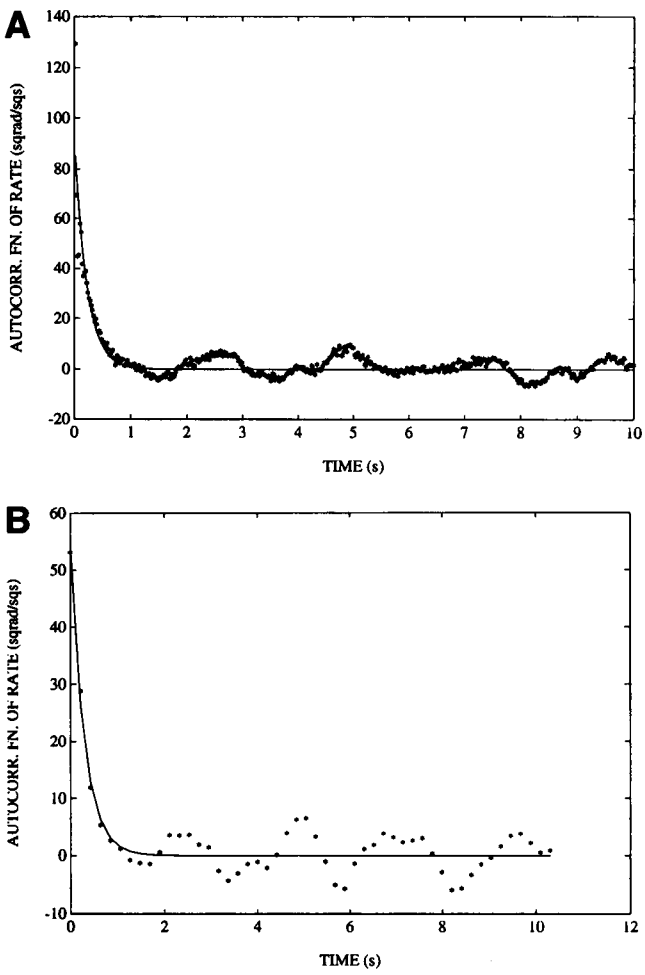

FIGURE 5 Autocorrelation function of the rotation rate of a tethered *E. coli* cell (RP1091). The data are for the first cell in Fig. 4. The autocorrelation function can be decomposed into the sum of two functions: an exponentially decreasing component and a low frequency component of period 2–3 s. (*A*) The best fit according to the equation $K(t) = K_0\exp(-t/T)$ (see text) gives the parameters $T = 0.21$ s and $K_0 = 93.66$ rad^2/s^2, leading to the value $D_\infty = 19.67$ rad^2/s. (*B*) Autocorrelation function of the rotation rate for the same cell averaged for each revolution. The best fit now gives the parameters $T = 0.29$ s and $K_0 = 53.90$ rad^2/s^2, leading to $D_\infty = 15.63$ rad^2/s.

peaks separated by 2- to 3-s time intervals. These peaks correspond to the low frequency oscillations described above in the section on slow changes in rotation rate. It is frequently assumed that the autocorrelation function has the exponential form $K(t) = K_0\exp(-t/T)$ in the high frequency range (Cooper and McGillem, 1967), where t represents time and K_0 and T are parameters. We approximated the initial fast component by this function. The best fit for most of the RP1091 cells studied was good, the coefficient of determination (see, for example, Ott, 1988) being $r^2 > 0.97$. The parameter K_0 corresponds to the variance of the local rotation rate σ^2_{loc} (calculated for the complete set of data), the parameter T to the memory of the system, i.e., the characteristic time during which the motor retains its rotation rate. The exponential best fit shown in Fig. 5 *A* gives the values $K_0 = 93.66$ rad^2/s^2 and $T = 0.21$ s for the initial component.

To check the stiffness of our results, we calculated the autocorrelation function of the rotation rate averaged through each revolution (as described in previous section) versus time. The exponential best fit shown in Fig. 5 *B* refers to the same cell and gives the values $K_0 = 53.90$ rad^2/s^2 and $T = 0.29$ s. The decrease in K_0 is a result of the averaging effect on the fluctuations. The agreement between the two autocorrelation functions confirms that we are dealing with motor properties and not with sampling artifacts.

Mean rotation rate

The hypothesis of Khan et al. (1985) that tethered cells are free to execute rotational Brownian motion is based on the assumption that the average rotation rate does not change significantly over relatively long time intervals. To verify the existence of a stable average rotation rate characteristic of each RP1091 cell, the dependence of the average revolution period for a given time interval was examined as a function of the length of this interval. An example is plotted in Fig. 6. After approximately 100 revolutions the curve reaches a plateau, after which changes in the mean revolution period do not exceed 3%. Another procedure was to fit a parabolic function to the time dependence of the accumulated angle to determine the sign and value of the coefficient of the square term. If a systematic decrease in rotation rate were present we would expect to obtain a statistically significant negative coefficient. This was not observed for the RP1091 cells studied. The same conclusion can be derived from the rate autocorrelation plots (see Fig. 5). Only cells

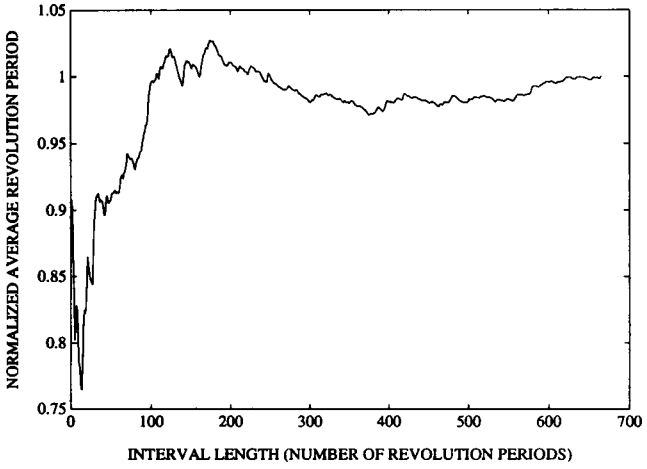

FIGURE 6 Dependence of the average revolution period for a given time interval as a function of the interval length. The data are normalized to the mean period of revolution in the plateau, 0.209 s (see text). Note that the asymptotic rise reflects the arbitrarily chosen zero time; a different choice of zero time for the same cell produces an asymptotic decrease to the same stable average. The interval between tethering and the start of data acquisition generally varied between several minutes and an hour.

clearly exhibiting a consistent mean rotation rate (varying by less than ±3%) were analyzed further.

Mean square residual angle and diffusion coefficient

From the accumulated angle $\theta(t)$ describing the position of the long axis of a tethered bacterium we obtain the average rate of rotation, $\overline{\omega(t)}$, and hence the residual accumulated angle $\Delta\theta(t)$:

$$\Delta\theta(t) = \theta(t) - \overline{\omega(t)}\, t\,. \tag{2}$$

According to the simple rotational diffusion model used by Khan et al. (1985), i.e., rotational Brownian motion superimposed on a stable average rotation rate, the mean square residual angle $\langle(\Delta\theta(t))^2\rangle$ (an ensemble average, as will be discussed below) should be proportional to time:

$$\langle[\Delta\theta(t)]^2\rangle = 2Dt\,. \tag{3}$$

It was shown by Einstein (1906) that the proportionality in Eq. 3 extends down to $\sim 10^{-7}$ s for micron size particles in water at room temperature. Beyond this lower limit we enter the so-called ballistic domain, where the residual mean square angle is proportional to t^2:

$$\langle[\Delta\theta(t)]^2\rangle \propto t^2\,. \tag{4}$$

This is because the extremely short time scale considered (comparable with the mean time between collisions of the particle with the solvent molecules) effectively eliminates collision averaging. The generalization of Eq. 3 for all times has been discussed, for example, by Uhlenbeck and Ornstein (1930). The ballistic domain is generally beyond the limit of resolution in diffusion measurements. However, in our case, as is shown in Appendix A, the observed exponential component of the autocorrelation function is consistent with a ballistic type of behavior extending to the time scale of milliseconds (cf. Eq. 10 of Uhlenbeck and Ornstein, 1930):

$$\langle[\Delta\theta(t)]^2\rangle = 2K_0T^2[t/T + \exp(-t/T) - 1]\,. \tag{5}$$

A possible mechanism for this behavior will be discussed below. Expansion of the right-hand side of Eq. 5 leads to

$$\langle[\Delta\theta(t)]^2\rangle = 2K_0T^2[t^2/2T^2 - t^3/6T^3 + \ldots]\,, \tag{6}$$

which reduces to Eq. 4 at sufficiently small values of t/T.

The time-dependent diffusion coefficient determined from the residual mean square angle is

$$D(t) = 1/2\,\frac{d}{dt}\langle[\Delta\theta(t)]^2\rangle = D_\infty[1 - \exp(-t/T)]\,, \tag{7}$$

where $D_\infty = K_0T$ is the limiting value of diffusion coefficient as $t \to \infty$.

At short times we can approximate $D(t)$ by

$$D(t) \approx D_\infty t/T = K_0 t\ (t \ll T)\,, \tag{8}$$

whereas at long times $D(t)$ approaches the stationary value we have just seen

$$D(t) \approx D_\infty = K_0T\ (t \gg T)\,. \tag{9}$$

To compare the predictions of this model with experimental data, we subtracted the component of the accumulated angle corresponding to a constant rotation rate from the data shown in Fig. 1 *A*. This gave rise to the residual angle shown in Fig. 7. Note that the slope of the linear component corresponds to the plateau of the average revolution period (see Fig. 6).

To calculate the mean square residual angle $\langle[\Delta\theta(t)]^2\rangle$, an ensemble for averaging must be defined that is large enough to provide a truly representative mean. To minimize the effect of the low frequency oscillations, the time interval corresponding to one sampling period should be significantly less than their characteristic time (2–3 s in the case of the bacterium depicted in Fig. 5). At the same time this time interval should exceed the value of T determined from the exponential fit of the autocorrelation function (0.21 s for this cell). These conditions were met (see Appendix C) by choosing the geometric mean of the characteristic times, T_m, as the sampling period (0.6 s in the case of Fig. 5).

The following algorithm was then used. The accumulated angle ($\theta(t)$) data for each bacterium were divided into successive intervals of the same length T_m. From the values of $\theta(t)$ in each interval the quantity $\overline{\omega(t)}t$ was subtracted (Appendix A, Eq. A2). The latter quantity incorporates the global mean rotation rate determined by the plateau in Fig. 6. The sets of residual angles $\Delta\theta(t)$ thus formed were brought to the same origin, as shown in Fig. 8. Each set was viewed as an independent realization of the stochastic process and the mean square of the residuals $\langle[\Delta\theta(t)]^2\rangle$ was calculated. A typical time dependence of the mean square residual angle value for a tethered RP1091 bacterium is shown in the upper curve of Fig. 9. This was obtained by

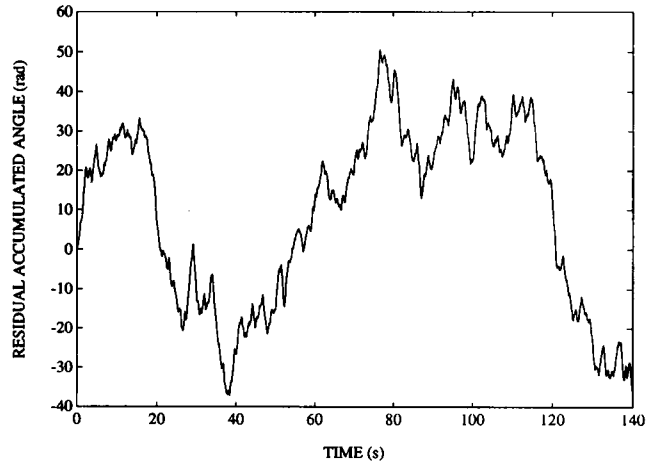

FIGURE 7 Residual accumulated angle as a function of time for a tethered *E. coli* cell (RP1091). The residual accumulated angle was obtained by subtracting the linear component (corresponding to rotation with a constant rotation rate) from the data depicted in Fig. 1 *A*.

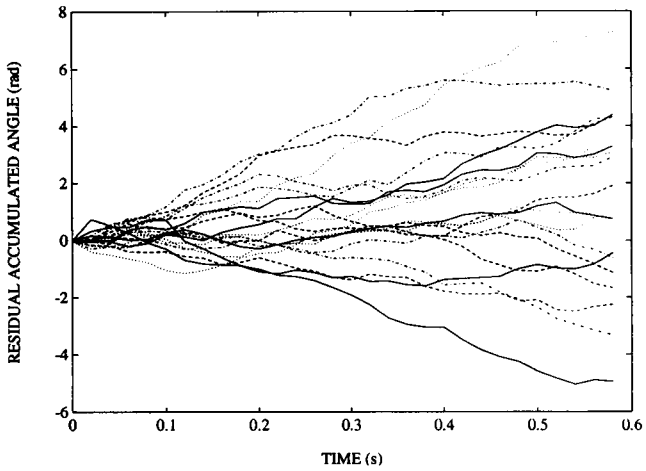

FIGURE 8 Residual accumulated angle as a function of time. The data were subdivided into 233 intervals and brought to the same origin. A group of 20 of these are depicted.

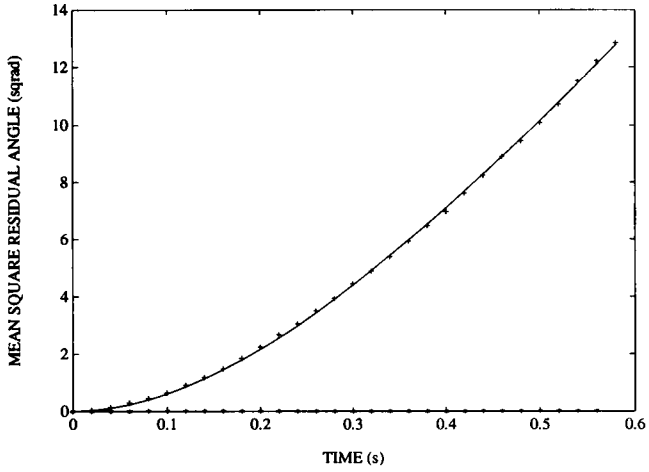

FIGURE 9 Mean square residual angle as a function of time. *Upper curve*: The mean square residual angle time dependence for an *E. coli* cell (RP1091), the first cell in Fig. 4, is characterized by a typical concave shape on a time scale of seconds. Averaging was done with 233 intervals. The number of intervals was chosen to produce an interval length of 0.6 s as discussed in the text. *Lower curve*: The mean square residual angle time dependence for an RP3098 cell of similar size attached to the cover glass by antibody against the cell surface. The diffusion coefficient is 0.02 rad^2/s.

averaging 233 sampling periods (so as to arrive at the value T_m = 0.6 s from the 6990 data points sampled at 20-ms intervals). Clearly, simple rotational diffusion (Eq. 3) cannot account for the data. The characteristic concave shape of the plot, followed by an approach to linear time dependence with increasing values of time, was seen in the majority of cells.

The best fit corresponding to Eq. 5 of the upper curve of Fig. 9 was good (r^2 = 0.999), yielding the values K_0 = 68.39 rad^2/s^2, T = 0.28 s, and $D_\infty = K_0T$ = 19.15 rad^2/s. Mean values (±SE) of the parameters D_∞ and T for 23 RP1091 cells (group 1) are given in Table 1. All of these cells were selected according to the criterion $r^2 \leq 0.99$ when fitting to the exponential region of the autocorrelation function. In this group the values of both D_∞ derived from residual mean square angles and $D_{\alpha=1}$ (not shown) derived from rotational periods significantly exceed the calculated value of D_f. Values of the same parameters for the remaining 7 RP1091 cells (group 2) are also given in Table 1. Here $r^2 < 0.99$ when fitting to the exponential region of the autocorrelation function, and the smaller mean value of T corresponds to a less pronounced concavity and hence a closer approach to simple rotational diffusion. Accordingly the D_∞ values are, on the average, closer to the D_f values. The broad spread of the values of D_∞ indicated by the relatively large SE shown in Table 1 probably reflects variations in the properties of individual motors and their local microenvironments.

The lower curve of Fig. 9 corresponds to the mean square angle calculated by the same algorithm for an RP3098 cell (a mutant lacking flagella as well as the chemotaxis machinery (Parkinson and Houts, 1982)) tethered to a cover glass by antibody against the cell surface. The cell jitters around its equilibrium position because of random collisions with the medium molecules. In the case of free rotational diffusion of a cell with the same geometry around a tether, we would expect a linear dependence of the mean square angle with a diffusion coefficient D_f = 0.2 rad^2/s. The value obtained from the lower curve of Fig. 9, 0.02 rad^2/s, is a result of the restriction imposed on the bacterial body by the antibody tethering it to the cover glass.

Point dark-field microscopy

In an attempt to discriminate between possible sources of the oscillations in rotation rate, point dark-field microscopy (Levin and Korenstein, 1991; Mittelman et al., 1991) was carried out. Light reflection and scattering from flagellated cells (RP1091) attached to a coverslip by antibody to the flagellin, and nonflagellated cells (RP3098) attached to a coverslip by antibody to the cell surface, were examined. Both strains produced low frequency oscillations characterized by a PSD similar to that shown in Fig. 2. These results suggest that low frequency oscillations are unconnected with the motor machinery and hence are probably related to local mechanical movements of the membrane.

Rapid changes in rotation rate: an interpretation in terms of dissociation and association of the force-generating units

The effect of changes in the number of force-generating units on motor rotation can be analyzed in terms of the following model. It is assumed that there are n independent units, each of which can exist in two states with respect to the rotor: associated and dissociated. Each associated unit contributes an additive component ω_0 to the rotation rate, whereas dissociated units do not contribute. Note that, in terms of the Berg-Khan or Läuger models, dissociated force-generating units would not be expected to conduct

protons (Caplan and Kara-Ivanov, 1993). Indeed, relatively low conductivity was observed in vesicles containing wild-type MotA, the protein postulated to be the proton-conducting component of the force-generating units (Blair and Berg, 1990). Even this low conductivity was later attributed to leakage stemming from an interaction with a fusion fragment generated by the plasmid used (Stolz and Berg, 1991). If the equilibrium probability of association for any given unit is p, one finds the expectation value and the mean square deviation of the rotation rate to be (see Appendix B)

$$\overline{\omega(t)} = np\omega_0 \tag{10}$$

$$\sigma^2 = np(1-p)\omega_0^2 . \tag{11}$$

From Eqs. 10 and 11 we obtain

$$p = 1/(1 + n[\sigma/\overline{\omega(t)}]^2) . \tag{12}$$

Making the simplest possible assumption that association of force-generating units occurs independently according to the equilibrium

$$\mathrm{F} + \mathrm{R} \rightleftharpoons \mathrm{FR} , \tag{13}$$

where F represents a dissociated force-generating unit, R the rotor (with or without other units bound), and FR the complex of both, we can write

$$p = [\mathrm{FR}]/([\mathrm{F}] + [\mathrm{FR}]) = k_1/(k_1 + k_2) . \tag{14}$$

Here k_1 is the pseudo-first-order rate constant for binding and k_2 the rate constant for release; hence at equilibrium

$$k_1[\mathrm{F}] = k_2[\mathrm{FR}] . \tag{15}$$

For the dimensionless dissociation constant K_d we have

$$K_d = k_2/k_1 = (1/p) - 1 . \tag{16}$$

As is shown in Appendix B the autocorrelation function of the rotation rate, $K(t)$, is in this case given by

$$K(t) = \sigma^2 \exp(-(k_1 + k_2)t) . \tag{17}$$

This means that the parameters of Eqs. 5 and 7 can immediately be identified with σ^2, $\sigma^2 T$, and $1/(k_1 + k_2)$, respectively:

$$K_0 = \sigma^2 , D_\infty = \sigma^2 T , T = 1/(k_1 + k_2) . \tag{18}$$

D_∞ can also be estimated as the integral of the autocorrelation function $K(t)$ (see Appendix A, Eq. A3) and σ^2 as the difference

$$\sigma^2 = \sigma_{\mathrm{loc}}^2 - \sigma_{\mathrm{sys}}^2 . \tag{19}$$

Hence the model predicts the characteristic early concavity and subsequent linearity in the residual mean square angle time dependence. From Eqs. 14 and 18 we obtain:

$$k_1 = p/T , \tag{20}$$

$$k_2 = (1-p)/T . \tag{21}$$

Estimation of the dissociation constant of a force-generating unit

The parameters n and ω_0 can be estimated from the data of Blair and Berg (1988): $n \approx 8$, $\omega_0 \approx 0.5$–1.9 Hz (for different cells). Mean values of p, k_1, and K_d for 23 RP1091 cells (group 1), calculated according to Eqs. 12, 16, and 20, are given in Table 2. In these calculations σ is approximated by σ_{loc}, as σ_{sys} is relatively small as indicated above in the section on rotation rate versus time. The values of ω_0 calculated from Eq. 10 are consistent with the eight steps in rotation rate observed by Blair and Berg (1988) on restoring defective motors. For this group of cells we find (mean value ± SE) $P = 0.49 \pm 0.04$, $k_1 = 2.19 \pm 0.34\ \mathrm{s}^{-1}$, $k_2 = 2.15 \pm 0.29\ \mathrm{s}^{-1}$, and $K_d = 1.51 \pm 0.27$. The number of force-generating units used in these calculations, $n = 8$, is close to the number of flagellar studs seen by electron microscopy (Khan et al., 1988). This number varied over a rather narrow range; complete ring structures had 14 to 16 particles in *Streptococcus* and 10–12 in *E. coli*. Note that, as the postulated dissociation-association reaction is stochastic, involving at least eight force-generating units, discrete changes in speed would not be expected to be resolved with our system.

The association of the force-generating units appears to be looser if n is taken to be larger than 8. The maximal value of n can be estimated from geometrical considerations. Assuming the diameter of the M ring to be 29 nm (Stallmeyer et al., 1989) and that of the MotA/MotB complexes to be 2.5 nm (based on the α-helix diameter given by Shulz and Schirmer, 1979), which supposedly correspond to the diameters of the rotor and force-generating units, respectively, the maximal number of the latter that can be fitted

TABLE 2 Calculated probabilities, rate constants, and dissociation constants of the force-generating units of RP1091 *E. coli* cells (group 1)

$n = 8$			$n = 25$		
p	k_1 (s^{-1})	K_d	p	k_1 (s^{-1})	K_d
0.49 ± 0.04	2.19 ± 0.34	1.51 ± 0.27	0.26 ± 0.03	1.21 ± 0.22	4.71 ± 0.88

Assuming n force-generating units in the motor, values of p (probability of a single unit being found in the associated state), k^1 (pseudo-first-order rate constant for binding of force-generating units), and K_d (dimensionless dissociation constant of force-generating units) were calculated according to Eqs. 12, 16, and 20. Mean ± SE (standard error of the mean) values are presented.

around the former is ≈40. However, such tight packing is obviously unlikely. Wilson and Macnab (1990) estimated the stoichiometry of MotB as 25 per flagellum, which is approximately the number of subunits in the M ring (Jones et al., 1990). Calculating as before for $n = 25$, we find (mean value ± SE) $P = 0.26 \pm 0.03$, $k_1 = 1.21 \pm 0.22\ s^{-1}$, $k_2 = 3.14 \pm 0.34\ s^{-1}$, and $K_d = 4.71 \pm 0.88$. In fact, as is clear from Eqs. 12 and 16, the value obtained for K_d is linearly proportional to the value of n assumed.

A minority of the cells (see Table 1, group 2) did not show the characteristic exponential phase of the autocorrelation function. In these cases the mean square residual angle versus time plot was significantly less concave, and the value of D_∞ was smaller and closer to that of D_f. We believe that these cells represent less usual cases in which the force-generating units are much more tightly associated with the rotor.

DISCUSSION

The main conclusion of this work is that the majority of tethered RP1091 cells do not behave according to a simple rotational diffusion model, i.e., their spinning cannot be described solely in terms of Brownian motion superimposed on a steady rotation. A slowly oscillating component, probably associated with local mechanical oscillations of the membrane and/or incomplete switching (see below), and a faster fluctuating component, possibly related to dissociation and association of the force-generating units, are common features of most of these cells. According to the minimal treatment consistent with both the Berg-Khan and Läuger models, a motor with eight force-generating units would require each unit to have a dimensionless (pseudo-first-order) dissociation constant of the order of 1.5 to account for the observed fluctuations. If the number of force-generating units is higher, the value of the dissociation constant is increased proportionately. Below we discuss these issues in more detail.

Comparison of the results of this study with those of earlier studies

Eisenbach et al. (1990) estimated the contribution of Brownian motion to fluctuations in rotation rate by using a visual frame-by-frame method on DNP-uncoupled bacteria and found it to be very small. However, such nonrotating bacteria may not have their motors in the same state as when rotating at physiological speeds. Instead, the motor may be located between two angular energy barriers, giving rise to partial or complete locking (Khan et al., 1985; Block et al., 1989). The simplest evidence for this is that DNP-treated cells do not usually drift at least one complete revolution in 6 min, which would be expected from free rotational diffusion according to Eq. 3 (cf. Berg, 1976).

Khan et al. (1985) observed an upward curvature in plots of the variance $\sigma^2_{\alpha\tau}$ in rotation interval versus the number of revolutions α per interval and attributed it to gradual changes in rotation speed over spans of ~1 min. An analytical expression for the influence of drift in rotation rate on the mean square angle time dependence is derived in Appendix C and shows that upward curvature is to be expected both in the case of a gradual decrease and in the case of a gradual increase of rotation rate. However, our results demonstrate the presence of upward curvature in cells rotating with constant mean rotation rates on time scales of 20–150 s. The upward curvature seen by Khan et al. (1985) in *Streptococcus* cells may well be a result, at least in part, of the low frequency oscillations in rotation rate we have found in *E. coli* cells. (The effect of such oscillations on the mean square angle is also discussed in Appendix C.) The use of autocorrelation analysis has enabled us to separate time scales and estimate D_∞. Indeed our analysis indicates that the limiting slope of the mean square angle time dependence approaches zero as $t \to 0$, so that the quantity $D_{\alpha=1}$ has some arbitrary intermediate value between zero and D_∞.

Plots of mean square displacement versus time with upward curvature have been referred to in the literature as "enhanced diffusion" (Klafter et al., 1992) and "directed motion" (Saxton, 1993). When followed by a linear region they reflect a type of extended ballistic regime that apparently characterizes the motor of RP1091 cells. The initial concave shape of the plot is related to the memory of the torque-generating machinery and is consistent with a model of associating and dissociating force-generating units. The high limiting diffusion coefficient D_∞ (see Table 1) evidently stems from high frequency fluctuations related to the mechanism.

Block et al. (1989) estimated the tether compliance from the autocorrelation function of angular jitter caused by Brownian rotation. They used partially locked *Streptococcus* cells (see above). Although the time constant determined by their method is of the same order of magnitude as those obtained in this work, the results are not related as the compliance cannot be a source of fluctuations. However, motor-generated torque fluctuations may well be partially damped by the tether compliance, leading to elevated values of T. In this case the calculated values of the rate constants k_1 and k_2 constitute lower limits, but K_d should not be substantially altered.

Possible sources of non-Brownian fluctuations in rotation rate

The possible sources of variations in the speed of rotation of tethered bacteria that are not attributable to Brownian motion can be divided into two major groups: (1) fluctuations not directly related to the motor, which include fluctuations in proton-motive force, interactions of the bacterial body with the glass surface including a non-uniform drag force distribution in the proximity of the surface, a possible modulation of the rotation by neighboring free-running motors

in the same bacterium, etc., and (2) fluctuations directly related to the motor, including both torque generation and switch action. Some of these sources are discussed below.

Fluctuation processes not directly related to the motor

Fluctuations in the driving force. The driving force of *E. coli* motors is the electrochemical potential difference of protons ($\Delta\mu_H+$) (reviewed in Caplan and Kara-Ivanov, 1993). Although both of its components, the membrane potential difference ($\Delta\psi$) and the difference in the proton concentration across the membrane (ΔpH), exhibit stochastic variations, the effect of fluctuations of $\Delta\psi$ (Läuger, 1984) and of ΔpH (Läuger, 1988) were estimated to be small. Manson et al. (1980) concluded that, for *Streptococcus*, $\Delta\mu_H+$ can be assumed constant for a metabolizing cell regardless of the dynamic load. Berg and Turner (1993) used the same assumption for *E. coli* cells. In our experiments $\Delta\mu_H+$ is unlikely to have changed significantly as the cells were in a motility medium rather than in a growth medium and at low density with adequate aeration.

Interactions with the glass surface. Cells interacting with the glass surface are expected to slow down or stop at fixed angles (Lapidus et al., 1988). However, only cells that did not exhibit a distinct slowdown at fixed angles were selected for the analysis described above. Hence, although we still cannot completely exclude interactions with the glass as a factor contributing to the fluctuations, they cannot be an important factor.

Fluctuation processes directly related to the motor

Association and dissociation of force-generating units. As already mentioned, the model of binding and release of force-generating units described above is consistent with the studies of Blair and Berg (1988) on the restoration of torque in defective flagellar motors. Although resurrected mutant cells show, for the most part, stable rotation in comparison with the predictions of our model, the conditions (e.g., intramembrane concentrations) are different from those described here and, furthermore, different mutants may vary significantly in their rate constants. It is interesting to note that Anazawa et al. (1992) and Shimizu et al. (1992) observed oscillations in their macroscopic measurements of tension and sarcomere length change in skeletal myofibrils and proposed that sarcomere length oscillation is connected with transitions of the cross-bridges between force-generating and non-force-generating states. Thus the fluctuations in rotation rate observed in our work may reflect an analogous intrinsic feature of the mechanism of torque generation.

Fluctuations in the proton occupancy of the force-generating units. A possible source of fluctuations is a variation in the number of protons in the proton channels constituting the force-generating units. This could result in apparent fluctuations of the driving force at constant $\Delta\mu_H+$. However, it was pointed out by Läuger (1988) that such fluctuations are likely to be strongly damped by elastic filtering. Kleutch and Läuger (1990) introduced a rotational diffusion coefficient accounting for fluctuations of force resulting from fluctuations in the occupancy of ion-binding sites. Stochastic simulations indicated that, under certain conditions, this quantity would increase with increasing protonmotive force although not enough to account for the high values of D_∞ observed in the present study (see Kleutch and Läuger, 1990, Fig. 16). However, such an effect might be related to the decrease of amplitude of the rate fluctuations we observed with increasing DNP concentration.

Sources of low frequency rate oscillations

Khan et al. (1985) observed that "from time to time, for no apparent reason, cells (*Streptococcus*) also rapidly shifted their rotation periods up or down by about 20 or 30%". Blair et al. (1991) mention "sudden speed changes that were occasionally seen" in *E. coli.* These reports concerning changes in the rotation rates of tethered bacteria may well be related to the low frequency oscillations seen in this study. In principle, such low frequency oscillations might arise from any perturbation affecting the force-generation geometry of the motor. We have focused on what seem to us the two most probable sources: incomplete switching and membrane oscillations.

Incomplete switching

The striking similarity between the time scales of the fast and slow phases in the rotation of RP1091 (gutted strain) cells and the clockwise and counterclockwise phases in RP437 cells suggests that the oscillations observed in RP1091 cells may be the result of incomplete switching of the motor. (The presence of an intact switch complex in RP1091 cells was demonstrated by Barak and Eisenbach, 1992.) If this is so, it implies that the switch undergoes autonomous transitions. Binding to the switch of CheY-P (the phosphorylated form of the chemotaxis protein CheY (Barak and Eisenbach, 1992)) or, to a lesser extent, of CheY itself increases the stability of the clockwise state of the switch and decreases the stability of the counterclockwise state of the switch. If CheY-P is not bound the outcome of the transition would be a decline in rotation rate. In other words, this notion implies that the initiation of switching is not the binding of CheY-P to the switch, as has been believed but is, rather, a built-in property of the switch itself; the binding of CheY-P enables the completion of the switching to occur. This feature can be readily incorporated into a model of the switch recently suggested by Macnab (1994), in which the tilt angle of FliM changes. Incomplete switching might involve additional tilt positions of FliM, and in some circumstances (e.g., in the presence of feedback) could conceivably become oscillatory rather than stochastic. Whether this is correct or not remains to be tested by more direct means.

Membrane oscillations

Mittelman et al. (1991) observed local submicron cell membrane displacements in B lymphocytes in the frequency range 0.3–15 Hz. Similar low frequency membrane oscillations in erythrocytes have been discussed by Levin and Korenstein (1991). In our case, studies with RP3098 cells suggest that mechanical oscillations in the plasma membrane probably occur. These may be responsible, at least in part, for the slow oscillations in rotation rate.

We thank R. Korenstein for the use of his point dark-field microscope and A. I. Burstein, A. M. Berezhkovskii, and L. Baranov for helpful discussions in treating the problems connected with mean square angle analysis.
This study was supported by the Basic Research Foundation administered by the Israel Academy of Sciences and Humanities.

APPENDIX

A: Autocorrelation function and mean square residual angle

The accumulated angle describing the position of the long axis of a tethered bacterium can be written as

$$\theta(t) = \int \omega(t)dt\,, \tag{A1}$$

where $\omega(t)$ is the rotation rate. From the experimentally determined accumulated angle time dependence, the average rate of rotation $\overline{\omega(t)}$ is obtained, and hence the residual accumulated angle $\Delta\theta(t)$ can be calculated:

$$\Delta\theta(t) = \theta(t) - \overline{\omega(t)}\,t = \int_0^t \Omega(t')dt'\,, \tag{A2}$$

where $\Omega(t) = \omega(t) - \overline{\omega(t)}$. It is seen that

$$\langle[\Delta\theta(t)]^2\rangle = \int_0^t\int_0^t \langle\Omega(t')\Omega(t'')\rangle > dt''dt' \tag{A3}$$

$$= 2\int_0^t\int_0^{t'} K(t' - t'')dt''dt'\,.$$

Here $K(t' - t'')$ is the autocorrelation function of the rate. For the exponential range of the autocorrelation function of the rate (see the section on autocorrelation function of rotation rate) we have

$$K(t) = K_0\exp(-t/T) \tag{A4}$$

and hence we find that

$$\langle[\Delta\theta(t)]^2\rangle = 2K_0T^2[t/T + \exp(-t/T) - 1]\,, \tag{A5}$$

which corresponds to Eq. 5.

B: Autocorrelation function and loose binding of force-generating units

To estimate the mean rotation rate and its variance as given in the section describing the model and its properties, we assume equilibrium binding of force-generating units. We first calculate the equilibrium probability distribution $W(m,n)$ where m units are associated and $n - m$ units are free. This is a well known problem (see, for example, Kittel, 1958). The probability of any given combination of m associated units and $n - m$ dissociated units is $p^m(1 - p)^{n-m}$; the required probability distribution $W(m,n)$ is therefore $p^m(1 - p)^{n-m}$ times the number of distinct realizations of m associated and $(n - m)$ dissociated units. As the number of such distinct realizations is $n!/[m!(n - m)!]$ we have

$$W(m\,,n) = n!p^m(1 - p)^{n-m}/[m!(n - m)!]\,. \tag{B1}$$

To calculate $\overline{\omega(t)}$ and σ^2, we assume that each force-generating unit acts independently of the others. For a single unit that can exist in two states the mean rate $\overline{\omega(t)}$ and variance μ^2 are given by

$$\overline{\omega_1(t)} = p\omega_0 \tag{B2}$$

$$\mu^2 = \overline{[\omega_1(t)]^2} - [\overline{\omega_1(t)}]^2 = p\omega_0^2 - p^2\omega_0^2 = p(1 - p)\omega_0^2\,. \tag{B3}$$

For n independent units these quantities should be proportional to n:

$$\overline{\omega(t)} = np\omega_0 \tag{B4}$$

$$\sigma^2 = n\mu^2 = np(1 - p)\omega_0^2\,. \tag{B5}$$

The above two equations correspond to Eqs. 10 and 11, respectively.

The autocorrelation function of the rotation rate $K(t)$ is given by (see Cooper and McGillem, 1967)

$$K(t) = \sum_{ij=0}^{n} [\omega_i - \overline{\omega(t)}][\omega_j - \overline{\omega(t)}]p_i p_{ij}(t)\,, \tag{B6}$$

where ω_i and ω_j are the rotation rates in states i and j, respectively, p_i is the equilibrium state probability, and $p_{ij}(t)$ is the conditional probability of a transition to state j from state i. Using the relations

$$\sum_i p_i p_{ij}(t) = p_j \text{ and } \sum_j p_j = 1\,, \tag{B7}$$

we obtain:

$$K(t) = \sum_{ij=0}^{n} \omega_i\omega_j p_i p_{ij}(t) - [\overline{\omega(t)}]^2\,. \tag{B8}$$

To calculate $K(t)$, we first calculate the autocorrelation function $K_1(t)$ corresponding to the association and release of one force-generating unit only. Using Eqs. B2, B3, and B8, and taking into account that the dissociated state does not contribute to rotary motion, we have

$$K_1(t) = \omega_0^2 pp_{11}(t) - [\overline{\omega_1(t)}]^2$$

$$= \omega_0^2 p(1 - p)\exp[-(k_1 + k_2)t] \tag{B9}$$

$$= \mu^2\exp[-(k_1 + k_2)t]\,,$$

where $p_{11}(t)$ is the conditional probability of remaining in the associated state, given by

$$p_{11}(t) = p + (1 - p)\exp[-(k_1 + k_2)t]\,. \tag{B10}$$

This conditional probability is obtained from the kinetics of a two-state system with appropriate initial conditions. The autocorrelation function $K(t)$ for n independent force-generating units is then

$$K(t) = nK_1(t) = n\mu^2\exp[-(k_1 + k_2)t] = \sigma^2\exp[-(k_1 + k_2)t], \quad \text{(B11)}$$

which corresponds to Eq. 17.

C: Influence of systematic changes in rotation rate on mean square angle

As indicated by Khan et al. (1985), a downward drift in rotation rate should lead to an increase in the concavity of the plot of variance in rotation interval versus number of revolutions per interval. The same is true for the mean square angle versus time dependence. In fact it is also true for an upward drift and indeed any systematic change in rotation rate from the mean value. Assume that, during a period of observation, T_{obs}, a small drift in rotation rate occurs that can be approximated by the linear correction γt (here γ is a constant coefficient of rate decrease):

$$\omega(t) = \omega_{init} + \Omega(t) + \gamma t, \quad \text{(C1)}$$

where ω_{init} is the initial rotation rate and $\Omega(t)$ is the random rate component (cf. Appendix A). The accumulated angle in this case will be (Eq. B1)

$$\theta(t) = \omega_{init}t + \Delta\theta(t) + \gamma t^2/2, \quad \text{(C2)}$$

and we can write an apparent mean square residual angle $\langle[\Delta\theta_{app}(t)]^2\rangle$ containing a correction term $A(t)$ as follows:

$$\langle[\Delta\theta_{app}(t)]^2\rangle = \langle[\omega_{init}t + \Delta\theta(t) + \gamma t^2/2 - \omega_{mean}t]^2\rangle = \langle[\Delta\theta(t)]^2\rangle + A(t), \quad \text{(C3)}$$

where ω_{mean} is the mean rotation rate in the time interval $0 - T_{obs}$, given by

$$\omega_{mean} = \theta(T_{obs})/T_{obs} = \omega_{init} + \gamma T_{obs}/2, \quad \text{(C4)}$$

and the term

$$A(t) = (\gamma t^2/2 + \omega_{init}t - \omega_{mean}t)^2 = \gamma^2(t^2 - T_{obs}t)^2/4 \quad \text{(C5)}$$

is nonnegative. This correction not only adds concavity to the mean square angle versus time dependence but also an inflection point. All this, of course, is a consequence of subtracting only the linear component of the rate, ω_{mean}, from the accumulated angle (see Eq. A2). Note that in the data analysis it is most important to subtract all regular rate components and thus leave only the random component. If some drift in rotation rate exists (no matter what the reason), the corrected residual angle should be employed.

It is of interest to calculate the effect of an independent periodic low frequency rate component on the residual mean square angle. After addition of the periodic component (for simplicity assumed to be sinusoidal with amplitude β, frequency λ, and phase ϕ) we have for the rotation rate

$$\omega(t) = \overline{\omega(t)} + \Omega(t) + \beta\sin(\lambda t + \phi). \quad \text{(C6)}$$

The accumulated angle in this case will be (Eq. A1)

$$\theta(t) = \overline{\omega(t)}\,t + \Delta\theta(t) + \beta[\cos\phi - \cos(\lambda t + \phi)]/\lambda. \quad \text{(C7)}$$

and subtracting only the component corresponding to rotation with constant rate, according to the algorithm described in the section on mean square residual angles and diffusion coefficients, leads again to an apparent mean square residual angle $\langle[\Delta\theta'_{app}(t)]^2\rangle$ given by

$$\langle[\Delta\theta'_{app}(t)]^2\rangle = \langle\{\Delta\theta(t) + \beta[\cos\phi - \cos(\lambda t + \phi)]/\lambda\}^2\rangle = \langle[\Delta\theta(t)]^2\rangle + (\beta/\lambda)^2\langle[\cos\phi - \cos(\lambda t + \phi)]^2\rangle = \langle[\Delta\theta(t)]^2\rangle + (\beta/\lambda)^2[1 - \cos(\lambda t)] \quad \text{(C8)}$$

(Note that this result can also be derived by substituting Eq. C6 into Eq. A1 and proceeding according to Eqs. A2 and A3.) The last term in Eq. C8 is the result of phase averaging, as the division into intervals as shown in Fig. 8 was performed without reference to the phase of any possible low frequency components. It contributes concavity on short time scales corresponding to oscillatory behavior. However, in our method of data treatment with T_m as the sampling period (see text) this term can be neglected for purposes of curve fitting; the use of Eq. 5 without adding the correction term is sufficiently accurate for our needs. Simulations with representative values of β and λ estimated from the autocorrelation curves (e.g., Fig. 5) show that the correction to the mean square residual angle never exceeds 5%.

REFERENCES

Anazawa, T., K. Yasuda, and S. Ishiwata. 1992. Spontaneous oscillation of tension and sarcomere length in skeletal myofibrils. *Biophys. J.* 61: 1099–1108.

Barak, R., and M. Eisenbach. 1992. Correlation between phosphorylation of the chemotaxis protein CheY and its activity at the flagellar motor. *Biochemistry.* 31:1821–1826.

Berg, H. C. 1974. Dynamic properties of bacterial flagellar motors. *Nature.* 249:77–79.

Berg, H. C. 1976. Does the flagellar rotary motor step? *In* Cell Motility, Vol. 3. R. Goldman, T. Pollard, and J. Rosenbaum, editors. Cold Spring Harbor Laboratory Press, Cold Spring Harbor, NY. 47–56.

Berg, H. C., and R. A. Anderson. 1973. Bacteria swim by rotating their flagellar filaments. *Nature.* 245:380–382.

Berg, H. C., and S. M. Block. 1984. A miniature flow cell designed for rapid exchange of media under high-power microscope objectives. *J. Gen. Microbiol.* 130:2915–2920.

Berg, H. C., M. D. Manson, and M. P. Conley. 1982. Dynamics and energetics of flagellar rotation in bacteria. *Symp. Soc. Exp. Biol.* 35: 1–31.

Berg, H. C., and L. Turner. 1993. Torque generated by the flagellar motor of *Escherichia coli. Biophys. J* 65:2201–2216.

Blair, D. F., and H. C. Berg. 1988. Restoration of torque in defective flagellar motors. *Science.* 242:1678–1681.

Blair, D. F., and H. C. Berg. 1990. The *Mot*A protein of *Escherichia coli* is a proton-conducting component of the flagellar motor. *Cell.* 60: 439–449.

Blair, D. F., D. Y. Kim, and H. C. Berg. 1991. Mutant *Mot*B proteins in *Escherichia coli. J. Bacteriol.* 173:4049–4055.

Block, S. M., D. F. Blair, and H. C. Berg. 1989. Compliance of bacterial flagella measured with optical tweezers. *Nature.* 338:514–518.

Caplan, S. R., and M. Kara-Ivanov. 1993. The bacterial flagellar motor. *In* International Review of Cytology: A Survey of Cell Biology, Vol. 147. K. W. Jeon and J. Jarvik, editors. Academic Press, San Diego, 97–164.

Cooper, G. R., and C. D. McGillem. 1967. Methods of Signal and System Analysis. Holt, Rinehart and Winston, New York, Chapter 10, 301-322.

Einstein, A. 1906. On the theory of Brownian movement. *Ann. der Physik.* 19:371–381.

Eisenbach, M., A. Wolf, M. Welch, S. R. Caplan, I. R. Lapidus, R. M. Macnab, H. Aloni, and O. Asher. 1990. Pausing, switching, and speed fluctuations of the bacterial flagellar motor and their relation to motility and chemotaxis. *J. Mol. Biol.* 211:551–563.

Iwazawa, J., Y. Imae, and S. Kobayasi. 1993. Study of the torque of the bacterial flagellar motor using rotating electric field. *Biophys. J.* 64: 925–933.

Jones, C. J., R. M. Macnab, H. Okino, and S.-I. Aizawa. 1990. Stoichiometric analysis of the flagellar hook-(basal-body) complex of *Salmonella typhimurium*. *J. Mol. Biol.* 202:575–584.

Khan, S., M. Dapice, and T. S. Reese. 1988. Effects of *Mot* gene expression on the structure of the flagellar motor. *J. Mol. Biol.* 202:575–584.

Khan, S., M. Meister, and H. C. Berg. 1985. Constraints on flagellar rotation. *J. Mol. Biol.* 184:645–656.

Kittel, C. 1958. Elementary Statistical Physics. Wiley, New York. 21–23.

Klafter, J., M. F. Shlesinger, G. Zumofen, and A. Blumen. 1992. Scale invariance in anomalous diffusion. *Philos. Mag. B.* 65:755–765.

Kleutsch, B., and P. Läuger. 1990. Coupling of proton flow and rotation in the bacterial flagellar motor: stochastic simulation of a microscopic model. *Eur. Biophys. J.* 18:175–191.

Kudo, S., Y. Magariama, and S.-I. Aizawa. 1990. Abrupt changes in flagellar rotation observed by laser dark-field microscopy. *Nature.* 346: 677–680.

Lapidus, I. R., M. Welch, and M. Eisenbach. 1988. Pausing of flagellar rotation is a component of bacterial motility and chemotaxis. *J. Bacteriol.* 170:3627–3631.

Läuger, P. 1984. Current noise generated by electrogenic ion pumps. *Eur. Biophys. J.* 11:117–128.

Läuger, P. 1988. Torque and rotation rate of the bacterial flagellar motor. *Biophys. J.* 53:53–65.

Levin, S., and R. Korenstein. 1991. Membrane fluctuations in erythrocytes are linked to MgATP-dependent dynamic assembly of the membrane skeleton. *Biophys. J.* 60:733–737.

Macnab, R. M. 1995. Flagellar switch. *In* Two-Component Signal Transduction. J. A. Hoch and T. J. Silhavy, editors. ASM Press, Washington, D.C. 181-199.

Manson, M. D., P. M. Tedesco, and H. C. Berg. 1980. Energetics of flagellar rotation in bacteria. *J. Mol. Biol.* 138:541–561.

Meister, M., and H. C. Berg. 1987. The stall torque of the bacterial flagellar motor. *Biophys. J.* 52:413–419.

Mittelman, L., S. Levin, and R. Korenstein. 1991. Fast cell membrane displacements in B lymphocytes. *FEBS Lett.* 293:207–210.

Ott, L. 1988. An Introduction to Statistical Methods and Data Analysis. PWS-Kent, Boston. 339.

Parkinson, J. S. 1978. Complementation analysis and deletion mapping of *Escherichia coli* mutants defective in chemotaxis. *J. Bacteriol.* 135: 45–53.

Parkinson, J. S., and S. E. Houts. 1982. Isolation and behavior of *Escherichia coli* deletion mutants lacking chemotaxis functions. *J. Bacteriol.* 151:106–113.

Ravid, S., and M. Eisenbach. 1983. Correlation between bacteriophage chi adsorption and mode of flagellar rotation of *Escherichia coli* chemotaxis mutants. *J. Bacteriol.* 154:604–611.

Sadron, C. 1953. Methods of determining the form and dimensions of particles in solution: a critical survey. *Prog. Biophys* 3:237–304.

Saxton, M. J. 1993. Lateral diffusion in an archipelago: single-particle diffusion. *Biophys. J.* 64:1766–1779.

Schulz, G. E., and R. H. Schirmer. 1979. Principles of Protein Structure. Springer Verlag, New York. 69.

Shimizu, H., T. Fujita, and S. Ishiwata. 1992. Regulation of tension development by MgADP and Pi without Ca^{2+}. *Biophys. J.* 61: 1087–1098.

Silverman, M., and M. Simon. 1974. Flagellar rotation and the mechanism of bacterial motility. *Nature.* 249:73–74.

Stallmeyer, M. J. B., S.-I. Aizawa, R. M. Macnab, and D. J. DeRosier. 1989. Image reconstruction of the flagellar basal body of *Salmonella typhimurium*. *J. Mol. Biol.* 205:519–528.

Stolz, B., and H. C. Berg. 1991. Evidence for interactions between MotA and MotB, torque-generating elements of the flagellar motor of *Escherichia coli*. *J. Bacteriol.* 173:7033–7037.

Uhlenbeck, G. E., and L. S. Ornstein. 1930. On the theory of the Brownian motion. *Phys. Rev.* 36:823–841.

Wilson, M. L., and R. M. Macnab. 1990. Co-overproduction and localization of the *Escherichia coli* motility proteins MotA and MotB. *J. Bacteriol.* 172:3932–3939.